MRS Advances © 2018 Materials Research Society
DOI: 10.1557/adv.2018.471

Molecular Packing-Dependent Exciton and Polariton Dynamics in Anthradithiophene Organic Crystals

Jonathan D B Van Schenck[1], Gregory Giesbers[1], Akash Kannegulla[1], Li-Jing Cheng[1], John E. Anthony[2], Oksana Ostroverkhova[1]

[1]*Oregon State University, Corvallis, OR, United States.*

[2]*University of Kentucky, Lexington, KY, United States.*

Abstract

Polarization-dependent absorption spectra of two functionalized derivatives of fluorinated anthradithiophene, diF TES-ADT and diF TDMS-ADT, were studied in the crystal phase using a Holstein-like Hamiltonian. For both molecules, the primary contribution to the lowest energy absorption was found to be the S_0-S_1 excitonic transition perturbed by an intermolecular coupling of 15 meV for both TES and TDMS. A secondary contribution, consistent with that from charge-transfer states, was also found. Additionally, absorption spectra were analysed when crystals were placed inside of optical microcavities formed by two metal mirrors. Cavities exhibited a primary absorption peak determined to be an enhanced absorption from the lowest-energy S_0-S_1 transition.

INTRODUCTION

Organic semiconductors (OSC) have long been an enticing alternative to inorganic SC because of the relative ease of processing and lower costs. Developments in the field have made OSCs closer to wider commercialization of their applications, enabled by demonstrations of charge carrier mobilities over 10 cm^2/Vs and power conversion efficiencies exceeding 10% [1]. Yet there are still open questions about the nature of excitonic states in OSCs, specifically how intermolecular interactions affect the excitonic states in the solid state, depending on the molecular packing [2].

Organic polaritonics, where OSC excitonic states are coupled to photon modes in an optical cavity, has also recently received much attention due to their promise of high performance photonic devices such as low-threshold polariton lasers [3]. However, the detailed structure of organic polariton states is not well understood, especially in organic crystals, due to the complicated interaction between excitonic, vibronic and light-matter coupling [4].

In this paper, we present an analysis of how intermolecular coupling affects the excitonic structure of two model molecular crystal systems and discuss its implications for optical properties of these materials in polaritonic devices. We focus on two functionalized derivatives of anthradithiophene (ADT): diF-TES-ADT (TES) and diF-

TDMS-ADT (TDMS) (Fig. 1(a)-(c)). Both TES and TDMS crystals have a triclinic crystal structure and one molecule per unit cell ($Z = 1$). TDMS has its two longest crystal axes approximately equal (a = 7.2 Å, b = 11.3 Å, c = 11.9 Å) leading to a "slip-stack" packing scheme. TES has its two shortest crystal axes approximately equal (a = 7.1 Å, b = 7.2 Å, c = 16.6 Å) leading to a "brickwork" packing scheme [5]. Since side groups such as TES or TDMS do not affect the spectra of isolated molecules [6], spectral differences between TES and TDMS crystals are principally due to molecular packing effects.

EXPERIMENTAL DETAILS

TES crystals were created by dropping 17 μL of 30 mM solution in chlorobenzene onto glass substrates. These drops were then covered and allowed to evaporate slowly at 5 °C over several hours. The crystallization process of TDMS was enhanced by marring the surface of the glass substrate with widely spaced (1 cm) vertical scores. These scores provided nucleation sites for crystallization. All optical measurements were taken on crystalline regions away from these substrate defects where the TDMS crystals had grown at least 1 mm into the clean portion of the substrate. Both derivatives produced long and thin finger-like crystals, with the short dimension between 20 and 60 μm. We will refer to the orientation of the long dimension as the long axis of the crystal (Fig. 1(d)).

Optical microcavities were created by first evaporating 100 nm of silver onto a glass substrate using a Veeco thermal evaporator. The silver surface was marred with a single score to enhance crystal growth. Crystals of TDMS solution from 1mM solution in chlorobenzene were grown. Another 20 nm of silver was then evaporated over the TDMS to finish the microcavity.

X-ray diffraction performed on TES and TDMS single crystals revealed a dominant (0l0) orientation (l = 1, 2, 3) for TDMS and (00l) (l = 1, 2, 3, 4) for TES crystals.

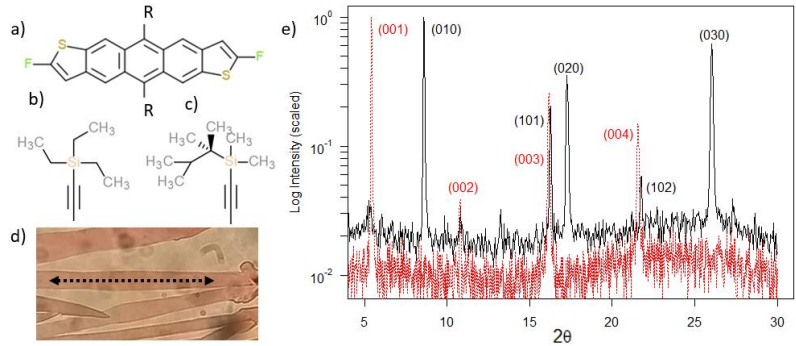

Figure 1: (a) Anthradithiophene molecule with R-groups (b) TES and (c) TDMS. (d) Optical image of a TES crystal with long crystal axis indicated with dashed line. (e) X-ray diffraction data for single crystals of TDMS (solid) and TES (dashed).

Optical properties of TES and TDMS crystals were studied using transmission- and reflection-based absorption setups utilizing the Olympus IX71 microscope. A fiber-coupled tungsten lamp provided a white light source that was first collimated, linearly polarized and then focused onto the sample from above (below) with a spot size

approximately 30 μm in diameter. Transmitted (reflected) light was analysed by an Ocean Optics USB2000 spectrometer.

For bare (cavity-free) crystals, absorption spectra were measured in transmission, in polarization increments of 10° between 0° and 180°, where 0° polarization was taken to be parallel to the long axis of the crystal. For the optical cavity, spectra were measured in reflection, in polarization increments of 30° between 0° and 120°. Example absorption spectra are shown in Fig. 2(a)-(b).

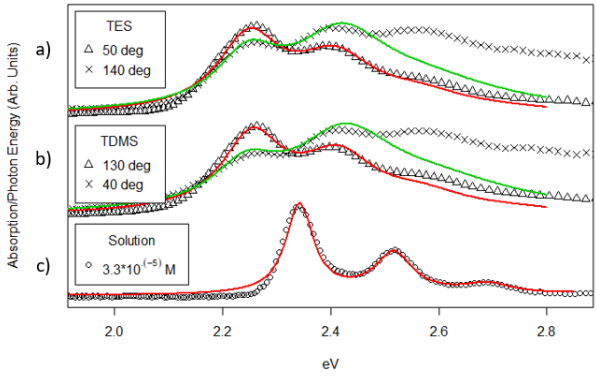

Figure 2: Normalized absorption spectrum for (a) a TES crystal, (b) a TDMS crystal and (c) TES in toluene solution. In (a)-(b), lines are linear combination fits: $\alpha S + \beta L$ as discussed in the text. For TES 50°: $(\alpha = 0.47, \beta = 0)$, for 140° $(0.04,\ 0.41)$, for TDMS 130° $(0.47,\ 0)$, for 40° $(0.10,\ 0.34)$. (c) Fit uses eq. 2 while setting $J_0 = 0$.

THEORY

We model both crystals with a Holstein-like Hamiltonian like that utilized by Spano [2]:

$$H = \sum_{n=1}^{N} E_X a_n^\dagger a_n + \sum_{n=1}^{N} E_V b_n^\dagger b_n + \sum_{n=1}^{N} E_V\left(\lambda\left(b_n^\dagger + b_n\right) + \lambda^2\right) a_n^\dagger a_n + \sum_{n=1}^{N}\sum_{m=1}^{N} J_{nm} a_n^\dagger a_m \qquad (1)$$

Here, n sums over all N molecule sites in the crystal, E_X is the exciton energy for TES (TDMS), E_V is the vibrational quantum of energy; $a_n^\dagger(a_n)$ and $b_n^\dagger(b_n)$ are the creation (annihilation) operators for undressed excitons and vibrational quanta respectively. λ^2 is the Huang-Rhys (HR) factor, and J_{nm} is the excitonic coupling matrix element between the nth and mth molecules.

By treating the excitonic coupling perturbatively, considering only nearest neighbour interactions, assuming $N \gg 1$ to apply periodic boundary conditions, and adopting Philpott's truncated basis [7], the absorption to first order can be expressed as:

$$A(\hbar\omega) = \alpha\,\hbar\omega \sum_{\tilde{\nu}} \frac{e^{-\lambda^2}\lambda^{2\tilde{\nu}}}{\tilde{\nu}!}\left|1 - 2J_0 \sum_{\tilde{\nu}\neq\tilde{\nu}'} \frac{e^{-\lambda^2}\lambda^{2\tilde{\nu}'}}{\tilde{\nu}'!\,(\tilde{\nu}' - \tilde{\nu})}\right|^2 \Gamma_{\sigma_0(1+\Delta\sigma\,\tilde{\nu})}\left(\hbar\omega - E_X - \left(\tilde{\nu} + 2J_0\frac{e^{-\lambda^2}\lambda^{2\tilde{\nu}}}{\tilde{\nu}!}\right)E_V\right) \qquad (2)$$

Here, J_0 is the ratio of the nearest neighbor coupling to the vibrational energy. The first term in the summand is the Frank-Condon factor for an unperturbed vibronic

progression, where the middle term characterizes the deviation induced by nearest neighbour coupling. The sum over vibrational quanta was truncated at a maximum value of $\tilde{\nu} = 4$, because the energy of states with $\tilde{\nu} > 4$ lie above the fitting region. To account for the spectral broadening observed in the absorption spectra, we assumed a Lorentzian lineshape for Γ together with a progressive linewidth $\sigma = \sigma_0(1 + \Delta\sigma\,\tilde{\nu})$, similar to that used in Ref. [5]. Further, the additional factor of $\hbar\omega$ was divided out, leading to a corrected vibronic progression lineshape with 7 parameters.

Fitting

Each of the 7 parameters predominately controls an independent feature of the total lineshape, except the HR factor λ^2 and the coupling ratio J_0 which both modulate the relative areas of the constituent Lorentzians. To mitigate this parameter degeneracy, absorption from dilute TES solution was fit with eq. 2 to find the value of the HR factor while assuming $J_0 = 0$. It was found that $\lambda^2 = 0.65 - 0.69$ (Fig. 2(c)). TDMS was assumed to have the same HR factor as TES, and so all crystal absorption measurements were fit with λ^2 fixed at 0.67, leaving only 6 independent parameters in eq. 2 (given in Fig. 3(b)).

Because the relative peak heights in polarization-dependent spectra of TES and TDMS varied greatly with polarization (shown in Fig. 2), we first explored the values of J_0 necessary to fit each polarization separately. It was found that no single value of J_0 was sufficient to fit all polarizations. Rather, J_0 smoothly transitioned between a minimum and maximum value (used in S and L described below). Because it is not physically reasonable for J_0 to depend upon polarization, we conclude that the absorption spectra cannot be due to a single vibrionic progression in the form in eq. 2, but are rather due to the superposition of at least two separate progressions each with a distinct (but fixed) intermolecular coupling value.

The TES and TDMS crystal spectra were modelled as the linear combination of two progressions of the form eq. 2 each with fixed parameter values. We denote the lineshape with the smaller intermolecular coupling as $S(\hbar\omega)$ and the larger coupling as $L(\hbar\omega)$; all parameter values are given in Fig. 3(b). The entire polarization-dependent absorption was then modelled as:

$$A(\theta, \hbar\omega) = \alpha(\theta)S(\hbar\omega) + \beta(\theta)L(\hbar\omega) \qquad (3)$$

Where α and β are the only parameters which vary with polarization (Fig. 3(a)).

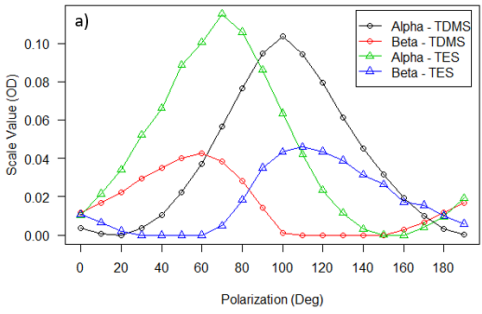

b)	S_{TDMS}	L_{TDMS}	S_{TES}	L_{TES}	$S_{Solution}$
J_0	0.095	0.53	0.094	0.50	0
λ^2	0.67	0.67	0.67	0.67	0.65
E_X	2.24 eV	2.16 eV	2.23 eV	2.17 eV	2.34 eV
E_V	160 meV	220 meV	160 meV	200 meV	170 meV
σ_0	140 meV	140 meV	140 meV	140 meV	62 meV
$\Delta\sigma$	0.25	0.70	0.26	0.70	0.41

Figure 3: (a) Plot of the scaling factors α and β used in the linear combination fits $\alpha S + \beta L$ for TES and TDMS. (b) Fit parameters for S and L lineshapes for TES and TDMS as well as for the TES solution fit with progressive broadening.

DISCUSSION

For both TES and TDMS, the linear combination fits for 50° and 130° respectively (in red in Fig. 2(a)-(b))—chosen to show S-like behaviour—follow the data points relatively well over the three lowest energy peaks, with only a slight underprediction of the heights of the third peaks. Throughout the polarization regions where the S contributions dominate (where $\alpha > \beta$—which is 20° to 110° for TES and 60° to 160° for TDMS), the fit similarly reproduces the lineshape seen in the spectra. This is in contrast with the linear combination fits for TES 140° and TDMS 40° (in green in Fig. 2(a)-(b))—chosen to show L-like behaviour. There is a large underestimation of the third (2.6 eV) peak. A similar deviation of the fit from the data is seen at other polarizations away from the S dominated polarizations. While the qualitative trend of the second peak is replicated by the fit, it does not exhibit the quantitative variation in peak height seen in the spectra. The different polarization dependence of the S and L contributions (shown as α and β in Fig. 3(a)) indicate that they have distinct physical origins.

We interpret the S contribution in TES and TDMS as the S_1 exciton manifold (seen in the solution spectra), perturbed by the intermolecular coupling J_0. The S_1 exciton should be the dominant contribution to the absorption, and Fig. 3(a) shows that the maximum value of α is a factor of 3 larger than that of β. The coupling ratio J_0 of $\sim$0.1 is comparable with calculations given in [8] on pentacene, where nearest neighbour coupling ratios ranged between 0.06 and 0.16 (with differing values due to the presence of translationally inequivalent molecules, Z = 2).

We interpret the L contribution as arising from states other than the S_1 exciton—possibly charge-transfer (CT) excitons. For polarizations where the state L dominates, the strongest absorption peaks are at $\sim$2.4 eV and $\sim$2.6 eV, suggesting that most of the states in L's manifold are more than 150 meV above the S_1 exciton energy. Other studies on similar molecules [8-10] have found CT states $\sim$200 meV above the S_1 exciton which yield absorptive features similar to those seen in TES and TDMS. CT states contributing to L would be consistent with L's distinct polarization dependence. Since eq. 1 does not explicitly include high energy CT states, modelling them with eq. 2 would require an artificially high value of J_0, functioning as an effective parameter, to shift the oscillator strength to higher energies. This could explain the large value of J_0 yielded by fitting as well as the model's deviation from the measured absorption above 2.6 eV.

Inside a microcavity, the TDMS oscillator strength shifts to favour the lowest energy peak, as seen in Fig. 4(a). The lowest energy peak follows the polarization-dependent trend of the bare (cavity-free) S contribution, exhibiting a minimum for polarizations near the long axis of the crystal and a maximum for polarizations near perpendicular. We attribute the lowest energy peak to the S_1 exciton. This corresponds to the S states in the bare TDMS crystals which are red-shifted by $\sim$0.11 eV in the cavity (Fig. 4(b)). The energy of this peak was similar for thicker regions of the same crystal, suggesting that the peak does not represent a fully hybridized exciton-photon (polariton) state.

The polarization trend of these absorption features from the cavity-clad TDMS crystals does not appear to follow the polarization dependence of the L contribution, suggesting it is not selected by the cavity. This also supports assigning L to CT states, because cavity modes are only expected to directly couple with Frenkel excitons (which have a considerably higher transition dipole moment than CT excitons). Similar results were obtained in TES optical cavities. Depending on the thickness of the crystal, additional peaks, interpreted as cavity resonances, appear in the spectra. Fig. 4(a) represents a thin crystal region where the first cavity mode is at energies above the shown region chosen to isolate the molecular response.

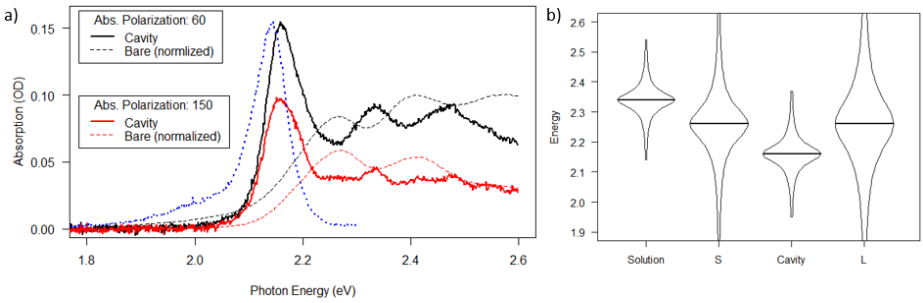

Figure 4: (a) Photoluminescence at 355 nm excitation (dotted) and polarization dependent absorption of TDMS in an optical cavity at normal incidence (solid). Normalized bare crystal absorption are included for comparison (dashed). (b) Energy diagram for the 0-0 peaks of solution and TDMS *S*, cavity and *L* with Lorentzian bounding shape taken from Fig. 3(b) and 4(a).

CONCLUSIONS

The polarization absorption spectra of TES and TDMS both exhibit evidence of a S_1 excitonic state with a vibronic progression (*S*) which is perturbed by intermolecular coupling of 15 meV for TDMS and TES. There is an additional contribution (*L*) to each absorption, possibly due to CT states. Finally, by comparing the bare crystal absorption to the absorption of crystals in an optical cavity, we observe that the primary low-energy feature in cavities corresponds to the lowest energy *S* contribution, which demonstrates that the cavity selectively interacts with the Frenkel exciton, rather than the states responsible for the *L* contribution to the spectra. Further work is necessary to confirm the nature of the latter and how the present observations extend to other molecular packing motifs.

ACKNOWLEDGMENTS

We thank A. Fox and Prof. B. Gibbons for the XRD measurements and the National Science Foundation (DMR 1207309 and DMR 1532225) for financial support.

References

1. Ostroverkhova, O. *Chem. Rev.* **116**, 13279–13412 (2016).
2. Spano, F. C. *Acc. Chem. Res.* **43**, 429–439 (2010).
3. Kéna-Cohen, S. and Forrest, S.R. *Nat. Phot.* **4**, 371 (2010).
4. Herrera, F. and Spano, F.C. *Phys. Rev. Lett.* **118**, 223601 (2017).
5. Jurchescu, O., Mourey, D. A., Subramanian, S., *et al. Phys. Rev. B* **80**, 85201 (2009).
6. Platt, A. D., Day, J., Subramanian, S., Anthony, J. E. & Ostroverkhova, O. *J. Phys. Chem. C* **113**, 14006–14014 (2009).
7. Philpott, M. R., *J. Chem. Phys.* **55**, 2039–2054 (1971).
8. Hestand, N. J., Yamagata, H., Xu, B., *et al. J. Phys. Chem. C* **119**, 22137–22147 (2015).
9. Qi, D., Su, H., Bastjan, M., Jurchescu, O.D., *et al. Appl. Phys. Lett.* **103**, 113303 (2013).
10. Yamagata, H., Maxwell, D.S., Fan, J., *et al. J. Phys. Chem. C* **118**, 28842 (2014).